14th Annual International Conference on Industrial Engineering and Operations Management
Dubai, United Arab Emirates (UAE), February 12-14, 2024
Publisher: IEOM Society International, USA DOI: 10.46254/AN14.20240316
Published: February 12, 2024

Vibration Analysis Based Analytical Reliability Model for Flexible-Coupling Pins with Parallel-Misalignment

Hussain VMS
Department of Mechanical and Manufacturing Engineering
National Institute of Advanced Manufacturing Technology,
Ranchi – 834 003. India
niffthussain@gmail.com

Naikan VNA
Professor, Subir Chowdury School of Quality and Reliability
Indian Institute of Technology, Kharagpur
Kharagpur – 721 302, India

Md. Israr Equbal
Mechanical Engineering Section, University Polytechnic,
Aligarh Muslim University, Aligarh-202 002, India

Abstract

This research paper introduces an innovative concurrent reliability computation model through experimentation, utilizing system vibration signals to address and minimize the adverse effects of misalignment on rotor system components. To assess reliability and understand the complex interplay, we present adapted design equations and employ a simulation-driven approach within the stress-strength interference paradigm. Furthermore, we suggest a framework to define secure and crucial thresholds for parallel misalignment and rotational speed, with the goal of achieving predetermined reliability objectives for flexible coupling pins. This model demonstrates efficacy in industrial rotor systems for regulating misalignment levels among components tailored to specific rotational speeds.

Keywords
Reliability, Flexible-coupling pin; parallel-Misalignment, Vibration analysis, Stress-Strength interference.

1. Introduction
Misalignment, the second most significant fault in rotating systems after mass imbalance, poses a considerable threat by generating vibrations that can result in system failure or catastrophic incidents (Desouki et al. 2020). This prevalent issue arises from various factors, including production defects, assembly tolerance variations, thermal distortions, dynamic piping forces, and foundation instability, leading to misalignments in forms such as parallel and angular misalignments, either individually or in combination.

To combat the challenges posed by rotor misalignment in rotating machinery, couplings play a crucial role as essential components, facilitating power transmission between drive and driven shafts without torsional slip (Haifei and Gong, 2019). Excessive misalignment in the coupling induces dynamic forces and moments, causing vibrations and

ultimately resulting in the failure of system components and the couplings themselves (Reddy and Shekar, 2015). In general, mechanically flexible couplings are preferred for their ability to accommodate misalignments and widely used in industries, especially for handling misalignments within specific intensity thresholds (Mancuso, 1999 and Xu and Marangoni, 1990).

The fault detection and identification of faults rotating systems, including misalignment, entail a comprehensive analysis of system signatures such as vibration, noise, thermal conditions etc. (Hussain and Naikan, 2013, 2016). Numerous fault detection methods are explored in the literature, with specific studies model forces generated by misalignments and analyzing their effects on system vibration and their patterns (Ran et al. 2019, Kumar and Tiwari 2023, Moysidis et al. 2023, Cao et al. 2018, Arumugam et al. 1995, Shekar and Prabhu 1995, Tadeo and Cavaca 2003, Jalan and Mohanty 2009, Bouchara et al. 2019, Samikannu and Basha 2012). The afore referenced research literature also showcases model-based diagnostic techniques for identifying faults in rotating systems, including misalignment and shaft cracks.

On the advent of faults, warranting the reliability of the entire system and its components is crucial for safety and sustained optimal performance. The reliability of the coupling, ensuring it performs its intended function, is vital for the overall reliability of the rotating system. While traditional design approaches often rely on safety margins, Dasgupta et al. (1995) propose a more sophisticated approach—the Stress-Strength Interference (SSI) model. This model treats stress and characteristic strength as random variables, offering a sophisticated and stochastic perspective on reliability. A concise survey of research works on SSI models is available in (Hussain and Naikan, 2012, 2013), justifying the selection of the SSI model for assessing the reliability of rotating systems/components in this paper.

Although theoretical models have been developed to address reliability and mass imbalance (Hussain and Naikan, 2012, 2013) there is a significant gap in validated experimental models specifically targeting reliability and misalignment in rotating systems. This paper aims to bridge this gap by introducing an experimental model crafted to measure the real-time reliability of a flexible coupling when misalignment occurs between drive and driven shafts. The findings of this research go beyond theoretical frameworks, offering practical applications to enhance reliability in industrial systems.

2. Proposed Model for Reliability Quantification

In this envisioned model, we employ the residual force generation technique from model-based fault diagnosis (Jalan and Mohanty 2009). This method is applied to assess the dynamic load imposed on the rotating system. The model under consideration utilizes the dynamic model information of a rotating system (Nelson and McVaugh, 1976). It calculates the dynamic force difference between the vibration signatures of a faulty and a faultless system, referred to as residual force.

2.1 Residual Force Generation

The vibrations generated in a faultless rotating system are represented by the linear equation of motion, involving the displacement vector $\mathrm{x}_o(t)$ at N degrees of freedom due to the functional/operational load $\mathrm{F}_o(t)$, as expressed in (1). The introduction of a fault, such as parallel misalignment in this scenario, leads to dynamic variations in the machine signature (i.e., vibration) within the system. The occurrence of the fault introduces additional load, resulting in changes in the vibration signature, as given in equation (2).

$$\mathrm{M}\ddot{\mathrm{x}}_0(t) + \mathrm{C}\dot{\mathrm{x}}_o(t) + \mathrm{K}\mathrm{x}_o(t) = \mathrm{F}_o(t) \quad (1)$$

$$\mathrm{M}\ddot{\mathrm{x}}(t) + \mathrm{C}\dot{\mathrm{x}}(t) + \mathrm{K}\mathrm{x}(t) = \mathrm{F}_o(t) + \Delta\mathrm{F}(t) \quad (2)$$

The magnitude of the vibration changes within the system is contingent on the fault type, severity, and location. The distinction in vibration signatures between the non-faulty and faulty systems results in the generation of residual displacement (equation 3), residual velocities (equation 4), and residual accelerations (equation 5).

$$\Delta\mathrm{x}(t) = \mathrm{x}(t) - \mathrm{x}_o(t) \quad (3)$$

$$\Delta\dot{\mathrm{x}}(t) = \dot{\mathrm{x}}(t) - \dot{\mathrm{x}}_o(t) \quad (4)$$

$$\Delta\ddot{\mathrm{x}}(t) = \ddot{\mathrm{x}}(t) - \ddot{\mathrm{x}}_o(t) \quad (5)$$

The equation for residual force (ΔF(t)) is derived by subtracting equation (1) from equation (2), as illustrated in equation (6), with the system matrices (M, C, and K) are constant. The constancy of system matrices in the residual force equation is grounded in the linear assumption made for the rotor system, in this model.

$$M\Delta\ddot{x}(t) + C\Delta\dot{x}(t) + K\Delta x(t) = \Delta F(t) \quad (6)$$

The determined residual force (ΔF(t)) is employed to determine the magnitude and location of the fault. To achieve an accurate calculation of the residual force attributable to the fault in the system, it is imperative to ensure identical operating conditions and vibration measurement conditions for both faultless and faulty rotating systems (Jalan and Mohanty 2009, Platz and Markert 2001).

2.2 Modal Expansion

To ascertain the residual vector (ΔF(t)) at all nodes of the system, it is imperative to obtain the residual vibration response (i.e., residual displacement, residual velocity, and residual acceleration) for all degrees of freedom (*N*) of the system. However, practical limitations often restrict the measurement of vibration response to only a few degrees of freedom (n), where n is considerably smaller than *N*.

To estimate the residual vibration response across all degrees of freedom from the measured residual vibration signature $\Delta x_n(t)$, the modal expansion technique is used (Pingle and Avitabile, 2011). This technique involves approximating the residual vibration as a linear combination of a limited number of eigenvectors ($\hat{\Phi}$). The complete residual vector $\Delta x(t)$ can be approximated by utilizing a reduced modal matrix ($\hat{\Phi}$), consisting of a set of mode shapes $\hat{X}_k$

$$\hat{\Phi} = [\hat{X}_1, \hat{X}_2, \ldots \hat{X}_k] \quad (7)$$

The maximum count of mode shapes within the reduced modal matrix $\hat{\Phi}$ should not exceed the number of independently measured vibration responses in $\Delta x_n(t)$, ensuring that K is less than or equal to n.
The measured residual vibration response $\Delta x_n(t)$ is connected to the full residual vector $\Delta x(t)$ through the utilization of the transformation matrix $(\tilde{T})$. This transformation matrix $\tilde{T}$ relies on the modal matrix $\hat{\Phi}$, and $\Delta x_n(t)$ is expressed as follows,

$$\Delta x(t) = \tilde{T}\, \Delta x_n(t) \quad (8)$$

In this proposed model, the System Equivalent Reduction Expansion Process (*SEREP*) is utilized to expand the available measured data $\Delta x_n(t)$. The *SEREP* expansion methodology utilizes the *SEREP* transformation matrix to extend the few measured degrees of freedom to cover all degrees of the system (Pingle and Avitabile, 2011). The *SEREP* transformation matrix is expressed as:

$$\tilde{T} = [\phi][\hat{\phi}]^g \quad (9)$$

Where $[\hat{\phi}]^g$ is given as,

$$[\hat{\phi}]^g = \left[[\hat{\phi}]^T \quad [\hat{\phi}]\right]^{-1} [\hat{\phi}]^T \quad (10)$$

Subsequently, substituting equation (8) into equation (6) results in expression (11), providing the estimated residual force at all degrees of freedom

$$M\tilde{T}\Delta\ddot{x}_n(t) + C\tilde{T}\Delta\dot{x}_n(t) + K\tilde{T}\Delta x_n(t) = \Delta F(t) \quad (11)$$

2.3 Operative Stress and Reliability Quantification

The additional dynamic load caused by misalignment must be estimated from the vector of equivalent load (ΔF(t)). Besides the design stress, for which the system/component is intended, the additional dynamic load resulting from misalignment will subsequently introduce an equivalent stress on the component/system. In the design equations of the components, particularly the flexible coupling pin in this instance, this additional stress needs to be integrated to determine the operative stress. The process of obtaining the operative stress is illustrated in Figure 1. Reliability quantification will be conducted using the operative stress.

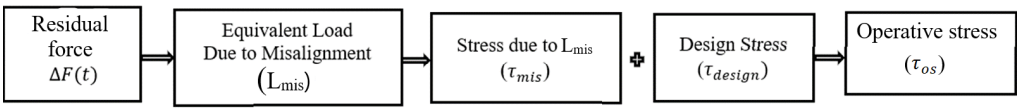

Figure 1. Flow chart for operative stress

The reliability quantification model employs the Stress-Strength Interference (SSI) failure model detailed in (Dasgupta et al. 1995, Kapoor and Lamberson, 1997). The SSI equation (12) below calculates the reliability of the component/system across a range of potential values for both the component/system strength (S_{TH}) and the stress (S_{ts}) induced by faults on the system.

$$R = \int_{-\infty}^{\infty} f_{S_{TH}}(S_{TH}) \left[\int_{-\infty}^{S_{TH}} f_{S_{ts}}(S_{ts})\, \mathrm{d}S_{ts} \right] \mathrm{d}S_{TH} \tag{12}$$

3. Illustration for the Analytical Reliability Model for Flexible Coupling Pin

This illustration focuses on the flexible coupling pin, delving into the design equations for the computation of shear and bending stresses. In an ideally aligned scenario, the coupling primarily encounters shear stress. But, misalignment, particularly parallel misalignment (excluding axial compression), introduces torque (T) and bending moments (M_b), giving rise to both shear and normal stresses on the coupling pins. To ascertain design stress (τ_{design}) encompassing both stress types (shear and bending), equations for Maximum Principal Stress and Maximum Shear Stress (15, 16) are employed. The recommended approach entails computing design stress using both equations and selecting the higher value to achieve an optimal coupling pin design.

The computation of shear stress and normal stress applied to the coupling hub is to be carried out using the following equations (13, 14).

$$\sigma = \frac{16}{\pi d_1^3} \times (P_b \times d_2 \times l) \times (l + 10) \tag{13}$$

$$\tau = \frac{4}{\pi d_1^2} \times (P_b \times d_2 \times l) \tag{14}$$

The maximum shear stress (15) of maximum normal stress (16) equations used in the design of coupling pin are given below in Figure 2,

$$\sigma_{design} = \frac{1}{2} \times \left(\sigma + \sqrt{\sigma + 4\tau^2} \right) \tag{15}$$

$$\tau_{design} = \frac{1}{2} \times \sqrt{\sigma + 4\tau^2} \tag{16}$$

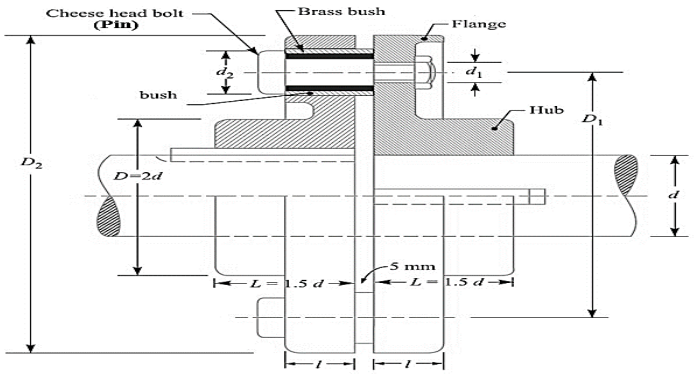

Figure 2. Flexible (bush-pin type) Coupling (Khurmi and Gupta, 2005)

The inclusion of the normal and shear stresses ($\sigma_{mis}\ and\ \tau_{mis}$) arising from parallel misalignment between the driven and drive shafts will yield the equations (17 and 18) for operative shear stress (τ_{os}) and operative principal stress (σ_{os}).

$$\sigma_{os} = \frac{1}{2} \times \left((\sigma + \sigma_{mis}) + \sqrt{(\sigma + \sigma_{mis}) + 4(\tau + \tau_{mis})^2} \right) \tag{17}$$

$$\tau_{os} = \frac{1}{2} \times \sqrt{(\sigma + \sigma_{mis}) + 4(\tau + \tau_{mis})^2} \tag{18}$$

The inherent parameters within the operative stress equations (17 and 18), encompassing dimensional attributes of coupling pins and the ultimate strength of the coupling pin material, exhibit stochastic characteristics stemming from manufacturing variations, operational influences, and environmental irregularities. This stochastic behavior introduces intricacy into reliability calculations, particularly when a substantial amount of field test data is impractical to obtain. Consequently, a simulation technique utilizing random number generation is employed to determine values for the random variables (Halder and Mahadevan, 2000), facilitating the computation of the operative stress on the coupling pin.

The generation of continuous random variables that align with their stochastic attributes and calculating outcomes for each realization within Equations 17 and 18, the operative stress values adopt a probabilistic nature. Likewise, the ultimate shear strength and ultimate normal strength for the shaft, dependent on the specific material type and shape, are generated to align with their stochastic properties.

The SSI equation (12) for reliability calculation mentioned earlier undertakes modification and expressed in (19) for the maximum shear stress model, while the maximum normal stress model is expressed in Equation (20). This adaptation facilitates a thorough assessment of the coupling pin's behavior when subjected to the additional shear and normal stress conditions, thereby enriching the analytical framework.

$$R = \int_{-\infty}^{\infty} f_{\sigma_{us}}(\sigma_{us}) \left[\int_{-\infty}^{\sigma_{us}} f_{\sigma_{os}}(\sigma_{os})\, \mathrm{d}\sigma_{os} \right] \mathrm{d}\sigma_{us} \tag{19}$$

$$R = \int_{-\infty}^{\infty} f_{\tau_{us}}(\tau_{us}) \left[\int_{-\infty}^{\tau_{us}} f_{\tau_{os}}(\tau_{os})\, \mathrm{d}\tau_{os} \right] \mathrm{d}\tau_{us} \tag{20}$$

In this subsequent section, the experimental work conducted on the test bed to measure resultant vibrations for stress calculations explained.

3.1 Experimental set-up and Procedure

The experimental process involves the acquisition of vibration responses using a machine fault simulator (MFS) experimental set-up, as depicted in Fig. 3a (schematically) and Fig. 3b (FEM model). The FEM model is divided into nine nodes, each having four degrees of freedom, encompassing two translational and two rotational motions, as detailed in (Shekar and Prabhu 1995, Nelson and McVaugh, 1976). Practical and cost considerations, discussed in section 2, determine that vibration response is recorded solely at node 3, located at the bearing-1 holder (Figure 3).

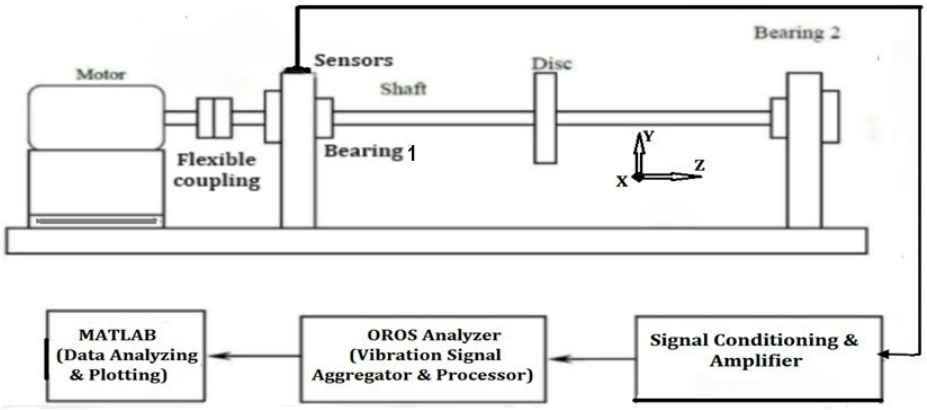

Figure 3a. Schematic diagram of experimental set-up

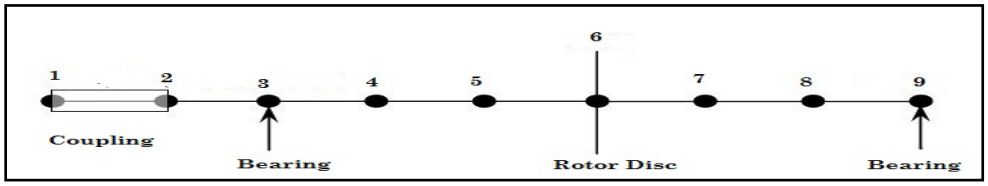

Figure 3b. FEM model of experimental set-up

For the collection of vibration data, we employ four ICP accelerometers with BNC connectors, operating within the 0.3 – 10 KHz range and delivering 100 mV/G sensitivity. Data collection and analysis are carried out using the OROS software, which uses digital integration to derive displacement and velocity amplitudes from the acquired acceleration data. MATLAB is utilized for data visualization and the software coding for analysis of data.

Vibration responses were recorded under both faultless conditions and with parallel misalignment, spanning from $0.254 \times 10^{-3}m$ to $1.016 \times 10^{-3}m$ at speeds ranging from 500 rpm to 8000 rpm. The rotational speed of the MFS is deliberately maintained below its first critical speed of 9000 rpm. Sample plots illustrating vibration responses are presented in Fig. 4 & 5 (faultless scenario) and Fig. 6 & 7 (with parallel misalignment).

The residuals vector, which comprises acceleration ($\Delta\ddot{x}(t)$), velocity ($\Delta\dot{x}(t)$), and displacement ($\Delta x(t)$), obtained under both faultless and parallel misaligned conditions, is fed into equation (11). This process involves the utilization of system matrices (**M**, C, and K) and the transformation matrix ($\widetilde{\mathrm{T}}$) to derive the residual force vector ($\Delta F(t)$) for all degrees of freedom. Assuming linearity in the system, there are no alterations in the system matrices. The resulting residual forces computed at different nodes of the testbed are visually represented in Figure 8.

3.2 Reliability Computation

The computation of reliability involves utilizing residual force and load exerted resulting from parallel misalignment to determine additional bending and shear stresses on the coupling pin, as outlined in section 2 and expressed in equations (13-18). These values, in conjunction with other relevant parameters, are input into equations (17, 18) to calculate operative stress values. In this scenario, following five-hundred thousand simulation cycles, the resultant values for random variables, namely operative shear stress (τ_{os}) and operative normal stress (σ_{os}), are fitted to suitable probability distributions. A comparable approach is applied to establish the distribution and parameters of ultimate strength. In this context, shear stress and ultimate shear strength are considered in the reliability calculation.

After the simulation cycles in this experimental work, both shear stress (τ_{os}) and ultimate shear strength (τ_{us}) values conform to a standard normal distribution. Integrating density functions into Equation (18) generates the reliability expression (21). Substituting the distribution parameters into equation (21) allows the determination of the coupling hub's reliability (Figure 4 and Figure 5).

$$R_{pin} = 1 - \Phi(z) \tag{21}$$

where $$z = \frac{(\mu_{\tau_{us}} - \mu_{\tau_{os}})}{\sqrt{(\varrho_{\tau_{us}})^2 + (\varrho_{\tau_{os}})^2}} \tag{22}$$

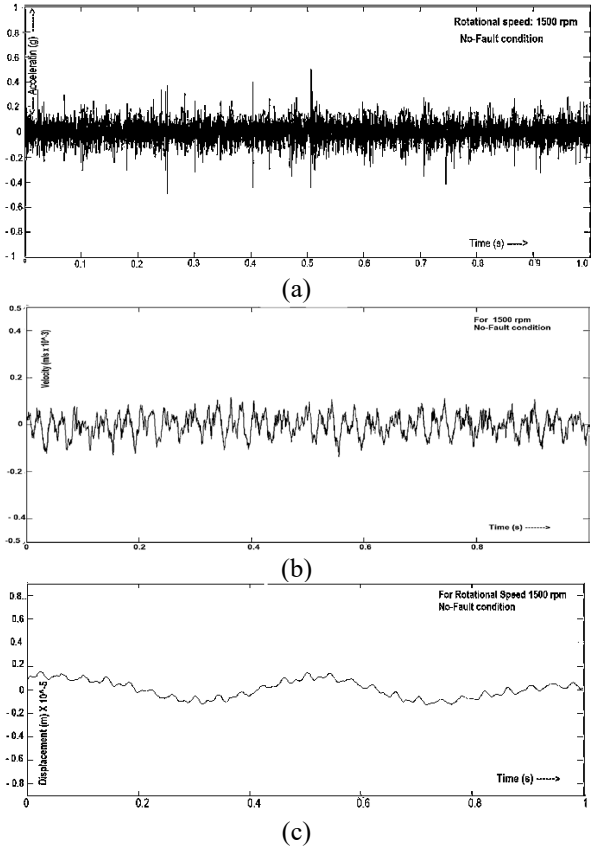

Figure 4. Vibration response (at bearing–nearer to coupling) in x-direction without faults for 1500 rpm rotor speed. Time-domain plots of (a) acceleration (b) velocity and (c) displacement

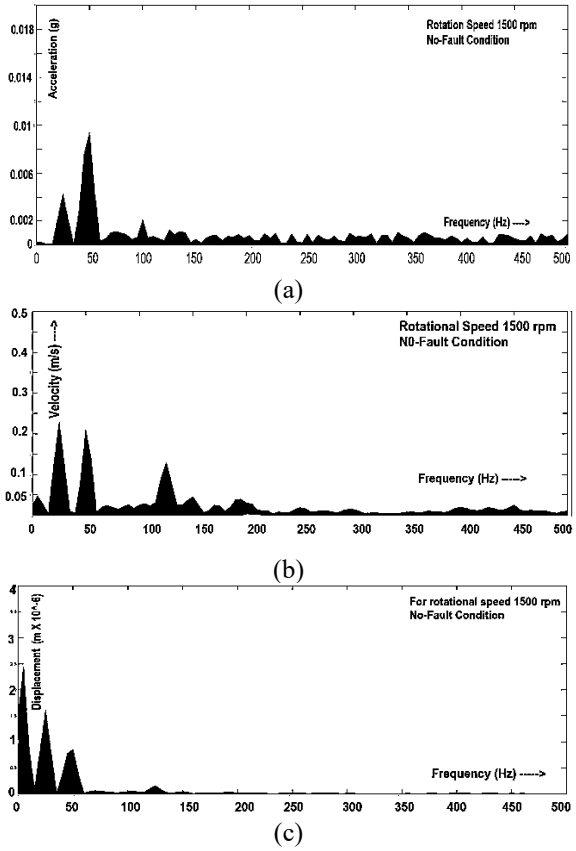

Figure 5. Vibration response (at bearing–nearer to coupling) in x-direction without faults for 25 Hz rotor speed. Frequency-domain plots of (a) acceleration (b)velocity and (c). displacement

3.3 Results of experimental work of illustration

The experimental methodology involved a process of iterative implementation, incorporating gradual adjustments in both parallel misalignment and rotational speeds. The vibration plots, showcased in Figures 4 to 7, unmistakably illustrate an increase in the vibration amplitude of the 2x running speed component, attributable to misalignment within the system (refer to Figure 7). An analysis of Figure 5, representing the faultless condition plot, reveals spikes in the 1x and 2x speed components, attributed to residual faults present within the system.

In Figure 8, the residual force plots for all nodes distinctly highlight misalignment, particularly at nodes 1 and 2, specifically within the flexible coupling. A comparative examination of the plots across incremental rotational speeds and parallel misalignment exposes a rise in residual force at the coupling with an increase in both rotational speed and misalignment.

Results from simulation cycles and the corresponding reliability of the coupling pin under varying misalignment (m) values and rotational frequencies (rpm) are tabulated in Table 1 and graphically represented in Figure 9. Analysis of experimental results implies that, within the experimental setup, parallel misalignment has a negligible impact on reliability on the coupling pin in the speed range of 25 Hz to 90 Hz. The reliability remains around 0.999 for the specified parallel misalignment range $0.254 \times 10^{-3}\ m$ to $1.016 \times 10^{-3}\ m$ at the given rotational speeds, indicating the safety in this misalignment and speed ranges in the utilized experimental setup. Subsequent analysis indicates a

discernible reduction in reliability at 95 Hz for all parallel misalignments exceeding $0.254 \times 10^{-3}\ m$, as illustrated in the reliability plots depicted in Figure 9.

Due to the experimental setup's inherent limitations that preclude life-testing, and to prevent irreversible damage to the testbed, the rotational frequency was restricted to a maximum of 95 Hz. It is noteworthy that the first critical speed of the test system is 150 Hz. To overcome the practical restrictions on the rotational frequency in this illustration, the regression analysis is used to extrapolate the obtained data to estimate the reliability of the coupling pin at higher rotational frequencies up to the first critical speed of 150 Hz.

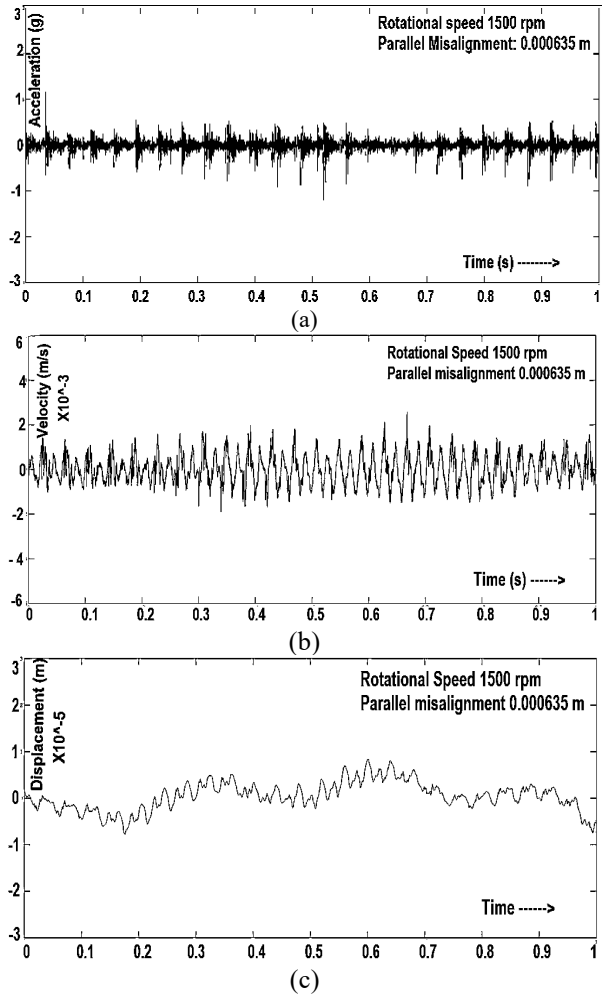

Figure 6: Vibration response (at bearing–nearer to coupling) in x-direction with parallel misalignment (ΔX=0.000635 m, ΔY= NIL) for 1500 rpm rotor speed. Time-domain plots of (a) acceleration (b) velocity and (c) displacement

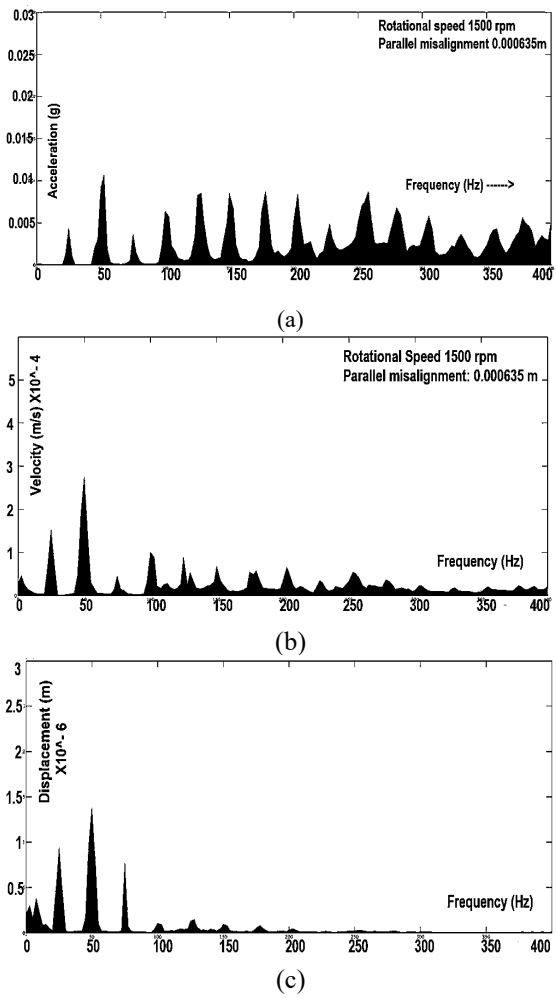

Figure 7: Vibration response (at bearing–nearer to coupling) in x-direction with parallel misalignment (ΔX=0.000635 m, ΔY= NIL) for 1500 rpm rotor speed. Frequency-domain plots of (a) acceleration (b) velocity and (c) displacement

The extrapolated reliability vs rotational frequency plots for various parallel misalignment have been given in figure 10. The examination of regression plots reveals a discernible decline in reliability as rotational frequency values increase. Nevertheless, within the parallel misalignment range of $0.254 \times 10^{-3}\ m$ to $1.016 \times 10^{-3}\ m$, reliability consistently remains above 0.999. This implies that the coupling pins exhibit a secure operational state up to the first critical speed (150 Hz) within the specified misalignment range. However, exceeding this range with higher rotational frequencies may result in decreased reliability and potential damage to subsystems/components in the rotating system. Consequently, real-time vibration monitoring is recommended, and corresponding maintenance tasks should be undertaken to ensure the system's safe operation (Table 1).

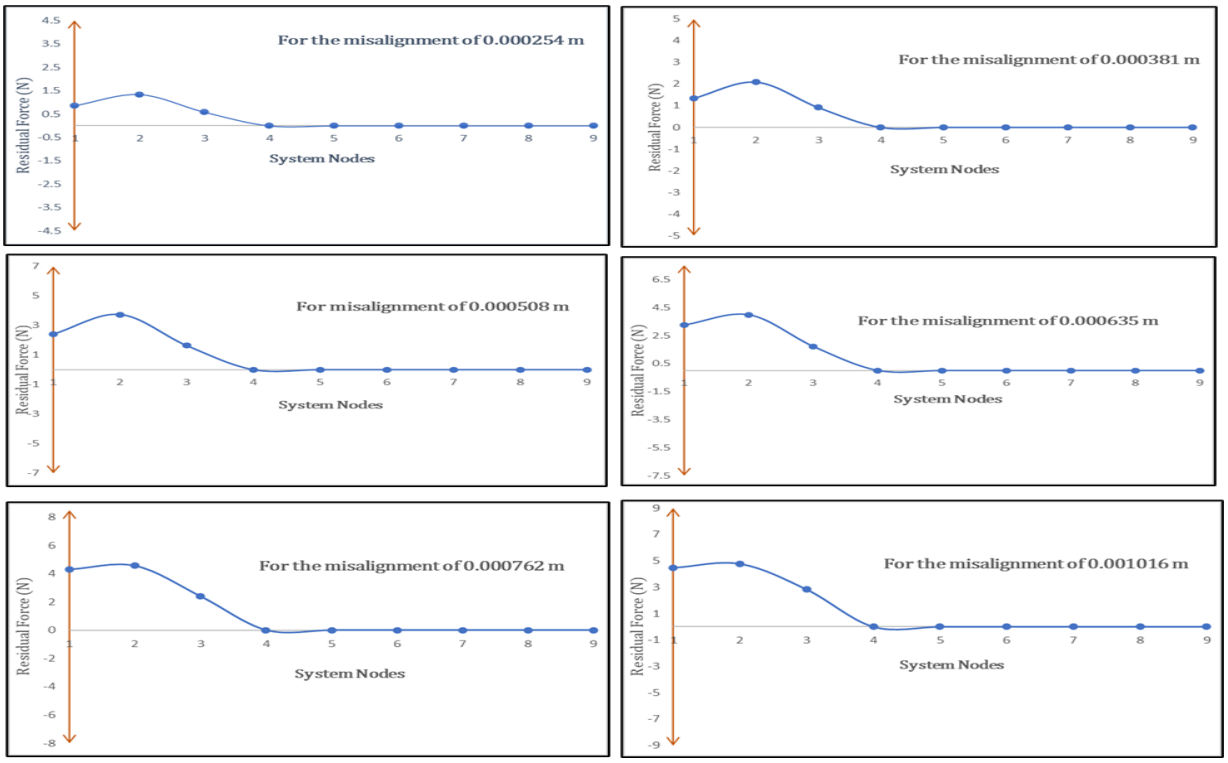

Figure 8. Residual force due to misalignment at a rotational frequency of 45 Hz at different nodes of test-bed

Table 1. Reliability values for different misalignment settings and rotational frequencies

Frequency ($\times 10^{-3}\ m$) → / **Misalignment (Hz) ↓**	**0.254**	**0.381**	**0.508**	**0.635**	**0.762**	**1.016**
25	0.999798	0.9997556	0.999754	0.999718	0.999765	0.99972
30	0.999777	0.9997518	0.999761	0.999717	0.999761	0.999718
40	0.999791	0.9997592	0.999752	0.999717	0.999748	0.999715
45	0.999785	0.9997531	0.999747	0.99971	0.99973	0.999703
50	0.999768	0.999753	0.999749	0.999714	0.999724	0.999697
60	0.999772	0.9997393	0.999742	0.999702	0.999716	0.999693
70	0.999737	0.9997312	0.999721	0.9997	0.99972	0.999682
80	0.999735	0.9996981	0.999685	0.999691	0.999716	0.999682
90	0.999708	0.9996907	0.999665	0.99968	0.99972	0.999674
95	0.999703	0.999685	0.999661	0.999674	0.999708	0.999654

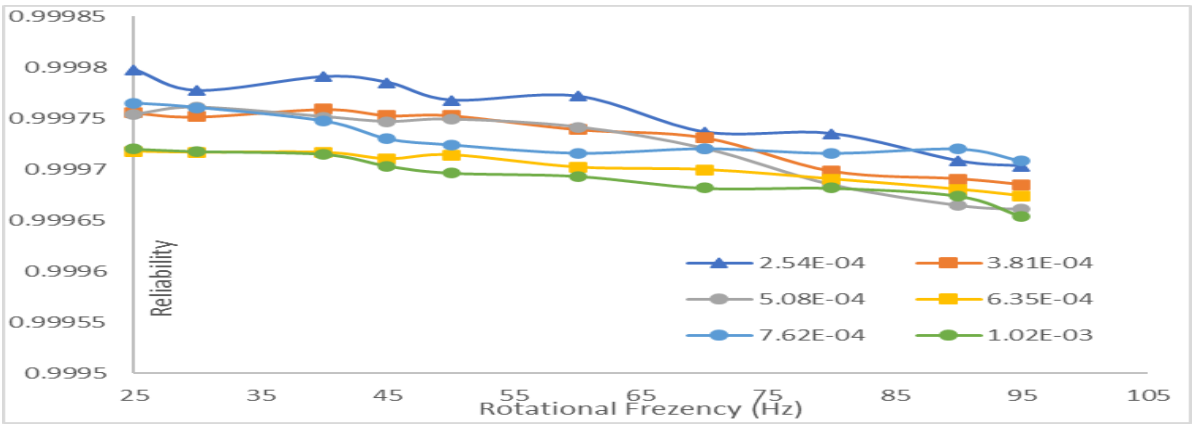

Figure 9. Reliability vs rotational frequencies (Hz) for different parallel misalignment (m)

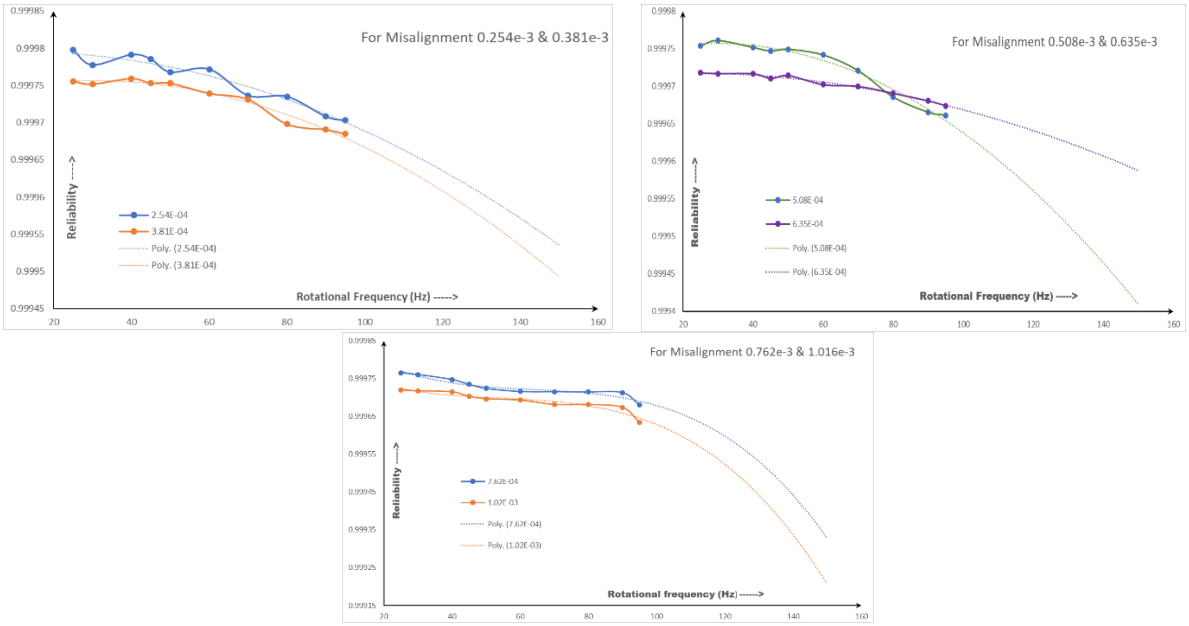

Figure 10. Regression plots for reliability Vs Rotational frequency for various parallel misalignment

4. Conclusion

An elevation in misalignment within rotating systems, particularly at elevated rotational speeds, gives rise to the generation of supplementary dynamic forces, potentially culminating in failures and catastrophic accidents. This research has introduced a real-time reliability model, leveraging the instantaneous vibration response, with a specific focus on coupling pins as an illustrative case. The efficacy of this model is evident in its ability to forecast the operational reliability of rotor systems affected by parallel misalignment through the measurement of vibration amplitudes. Tailoring the model to a specified reliability level enables the establishment of secure operational speed ranges for both existing and newly developed rotating systems.

As a prospective avenue, further reliability models could be developed through an experimental approach, concentrating on alternative faults within rotating systems and critical components thereof. This approach extends the utility of the model, making it applicable to a broader spectrum of scenarios and contributing to enhanced safety and reliability in various technological applications.

Notions:

M	:	Mass matrix
C	:	Damping matrix
K	:	Stiffness matrix
$\ddot{\mathrm{x}}_0(t)$	:	Acceleration vector of fault-free rotor system
$\dot{\mathrm{x}}_o(t)$	:	Velocity vector of fault-free rotor system
$\mathrm{x}_o(t)$	:	Displacement vector of fault-free rotor system
$\mathrm{F}_o(t)$	:	Force vector of fault-free rotor system
$\ddot{\mathrm{x}}(t)$	:	Acceleration vector of faulty rotor system
$\dot{\mathrm{x}}(t)$	:	Velocity vector of faulty rotor system
$\mathrm{x}(t)$	:	Displacement vector of faulty rotor system
$\Delta\mathrm{F}(t)$	:	Residual force vector
$\Delta\mathrm{x}(t)$	:	Residual displacement vector
$\Delta\dot{\mathrm{x}}(t)$	:	Residual velocity vector
$\Delta\ddot{\mathrm{x}}(t)$	:	Residual acceleration vector
n	:	Measurable degrees of freedom
N	:	All degrees of freedom
$\Delta\mathrm{x}_n(t)$	:	Measured residual vector
$\widetilde{\mathrm{T}}$	:	Transformation matrix
$\widehat{\Phi}$	:	Reduced modal matrix
$\widehat{\mathrm{X}}_1, \widehat{\mathrm{X}}_2, \ldots \widehat{\mathrm{X}}_k$	:	Mode shapes
$\Delta\mathrm{q}(t)$	:	Modal coordinate vector
$[\,]^T$	:	Transpose
L_{mis}		Equivalent Load due to misalignment
R	:	Reliability
S_{ts}	:	Stress in the coupling-hub
S_{TH}	:	Strength of the coupling-hub
$f_{S_{ts}}(S_{ts})$	:	Probability density function of stress
$f_{S_{TH}}(S_{TH})$	:	Probability density function of strength
τ	:	Shear stress
σ	:	Normal/bending stress
P_b	:	Bearing pressure on the pin
d_1	:	Diameter of the pin
d_2	:	Diameter of the bush
l	:	Length of the bush in the flange of the coupling
σ_{design}	:	Maximum normal stress
σ_{mis}	:	Normal stress due to misalignment
τ_{mis}	:	Shear stress due to misalignment
τ_{design}	:	Maximum shear stress
M_b		Bending moment
T	:	Torque
σ_{os}	:	Operative principal stress
τ_{os}	:	Operative shear stress
τ_{us}	:	Ultimate shear strength
σ_{us}	:	Ultimate normal strength
$f_{\sigma_{us}}(\sigma_{us})$	:	Density function of ultimate normal strength
$f_{\tau_{us}}(\tau_{us})$	:	Density function of ultimate shear strength
$f_{\tau_{os}}(\tau_{os})$	:	Density function of operative shear stress
$f_{\sigma_{os}}(\sigma_{os})$	:	Density function of operative normal stress
R_{pin}		Reliability of the coupling pin
$\Phi(z)$	:	Standard cumulative normal distribution function
$\mu_{\tau_{us}}$	:	Mean of ultimate shear strength

$\varrho_{\tau_{us}}$: Standard deviation of ultimate shear strength
$\mu_{\tau_{os}}$: Mean of operative shear strength
$\varrho_{\tau_{os}}$: Standard deviation of operative shear strength

References

Arumugam, P.; Swarnamani, S.; Prabhu, B. S. Effects of coupling misalignment on the vibration characteristics of a two-stage turbine rotor, *ASME Design Engineering Technical Conferences*. 84, 1049-1054, 1995.

Bouchra A.; Ali, E.; Hassan G. Experimental study on energy consumption in rotating machinery caused by misalignment, *SN Applied sciences*, 2, 1215, 2019.

Cao, H., Niu, L., Xi, S. and Chen, X. Mechanical model development of rolling bearing-rotor systems: A review. *Mechanical Systems and Signal Processing*, 102, pp.37-58, 2018.

Dasgupta, A., and M. Pecht, Material Failure Mechanisms and Damage Models. *IEEE Transactions on Reliability*, 40 (5), 531-536, 1991.

Desouki, M., Sassi, S., Renno, J. and Gowid, S.A. Dynamic response of a rotating assembly under the coupled effects of misalignment and imbalance. *Shock and Vibration*, pp.1-26, 2020.

Haifei, W., Gong, J. Dynamic analysis of coupling misalignment and unbalance coupled faults, *Journal of low frequency noise vibration and active control*. 38 (2), 1-4, 2019.

Halder, A., and S. Mahadevan, *Reliability Assessment Using Stochastic Finite Element Analysis. John Wiley*, New York, 2000.

Hussain VMS, Naikan VNA. Vibration Response Based Reliability Modeling for Rotor Systems with Imbalance. *International Journal of Performability Engineering*, 12(3), p.283, 2016.

Hussain VMS; Naikan VNA, Reliability modeling of rotary systems subjected to imbalance. *International Journal of Performability Engineering*, 9(4), p.423, 2013.

Hussain, V.M.S. and V.N.A. Naikan, Reliability and Imbalance Modeling of a Low-Pressure Turbine Rotor. *International Journal of Life Cycle Reliability and Safety Engineering*, 1 (2), 61-70, 2012.

Jalan, A. K.; Mohanty, A. R. Model based fault diagnosis of a rotor bearing system for misalignment and unbalance under steady state condition, *Journal of Sound and Vibration*. 327, 604-622, 2009.

Jamshidi, H., Jafari, A.A. and Jamshidi, P. Vibration behavior of misaligned rotor with the asymmetric shaft using Timoshenko beam theory. Scientia Iranica, 30(4), pp.1265-1278, 2020.

Kapoor, K.C., and L.R. Lamberson, *Reliability in Engineering Design. John Willey*, New York, 1997

Kumar, P. and Tiwari, R. A review: multiplicative faults and model-based condition monitoring strategies for fault diagnosis in rotary machines. *Journal of the Brazilian Society of Mechanical Sciences and Engineering*, 45(5), p.282, 2023.

Kurmi, R.S., and Gupta J., *A Textbook on Machine Design. Eurasia publishing House Lt.,* New Delhi, 2005.

Mancuso, J.R., Couplings and Joints: design, selection & application. *CRC Press,* 1999.

Moysidis, D.A., Karatzinis, G.D., Boutalis, Y.S. and Karnavas, Y.L. A Study of Noise Effect in Electrical Machines Bearing Fault Detection and Diagnosis Considering Different Representative Feature Models, *Machines*, 11(11), p.1029, 2023.

Nelson, H.D., and J.M. McVaugh, The Dynamics of Rotor-Bearing Systems Using Finite Elements. Transactions of ASME - *Journal of Engineering for Industry*, 98 (2), 593-600. 18, 1976.

Pingle P, and Avitabile P. Prediction of full field dynamic stress/strain from limited sets of measured data, *Structural Dynamics*, Volume 3. Springer, New York, 2011

Platz, R., and R. Markert, Fault Models for On-line Identification of Malfunctions in Rotor System. *Transactions of Fourth International Conference on Acoustical and Vibratory Surveillance*, Senlis, France, 435–446, 2001.

Ran, Y., Zhou, X., Lin, P., Wen, Y. and Deng, R., A survey of predictive maintenance: Systems, purposes, and approaches. *arXiv* preprint arXiv:1912.07383, 2019.

Reddy, M.C.S.; Sekhar, A.S. Detection and monitoring of coupling misalignment in rotors using torque measurements, *Measurements*, 2019.

Samikkanu, N.; Basha, A. M. J. Effects of misalignment of high-speed flexible coupling on the fighter aircraft transmission characteristics, *International Journal of Fluid machinery and Systems*. 5 (2), 91-99, 2012.

Sekhar, A. S..; Prabhu, B. S. Effects of coupling misalignment on vibration of rotating machinery, *Journal of Sound and Vibration*. 185 (4), 655-671, 1995.

Sudhakar, G. N. D. S.; Sekhar A. S. Coupling misalignment in rotating machines: modeling, effects and monitoring, *Noise and Vibration Worldwide*. 40 (1), 17-39, 2009.

Tadeo, A. T.; Cavalca, K. L. A comparison of flexible coupling models for updating in rotating machinery response, *Journal of the Brazilian society of mechanical science and engineering*. 25 (3), 235-246, 2003.
Xu, M.; Marangoni, R. D. Flexible couplings: study and applications, *Shock and Vibration Digest*. 22 (9), 3-11, 1990.

Biographies

Naikan VNA (Prof. Vallayil N. Achutha Naikan) is a professor in S.C. School of Quality & Reliability, and Department of Industrial Systems Engineering of Indian Institute of Technology, Kharagpur. He obtained his M.Tech. and Ph.D. in the reliability engineering from Indian Institute of Technology, Kharagpur. He has authored several research papers and books. His area of research includes mechanical system reliability, SPC, system dynamics simulation, and fault diagnosis. He has experience in working with University of Maryland, USA, the Chinese University of Hong Kong, Indian Space Research Organization, IIM, Ahmedabad and Union Carbide Calcutta. He is member of several professional societies and in the editorial board of several reputed research journals.

Hussain VMS (Prof. V. M. Shafiullah Hussain) is an assistant professor (Senior Grade) at the National Institute of Advanced Manufacturing Technology, Ranchi. He is a graduate in Mechanical Engineering from Vellore Institute of Technology (University of Madras) and holds a Master's degree in Production Engineering from Annamalai University. Additionally, he earned his Ph.D. in Reliability Engineering from the S.C. School of Quality & Reliability at IIT Kharagpur. He has authored several research papers and a book chapter. Furthermore, he is the holder of a U.K. design patent. His research interests encompass reliability modelling, vibration analysis for reliability quantification, Adaptive FMEA for manufacturing processes, Additive Manufacturing, and data analytics.

Md. Israr Equbal is an associate professor at mechanical engineering section, university polytechnic, Aligarh Muslim University, Aligarh. He obtained his M.Tech. and Ph.D. in manufacturing engineering from National Institute of Advanced Manufacturing Technology, Ranchi. He has authored several research papers in reputed journals such as CIRP etc. and book chapters. He is an organizer of many international and national level conferences. His area of research includes modelling and simulation, analysis and optimization of manufacturing process parameters, SPC and AI.